Investigation of magnetism and magnetic structure of anti-ThCr2Si2-type Tb2O2Bi by magnetization and neutron diffraction measurements

著者	Hideyuki Kawasoko, Kenji Ohoyama, Ryosuke Sei, Kota Matsumoto, Daichi Oka, Akinori Hoshikawa, Toru Ishigaki, Tomoteru Fukumura
journal or publication title	AIP Advances
volume	9
page range	115301
year	2019-11-08
URL	http://hdl.handle.net/10097/00130719

doi: 10.1063/1.5126399

AIP Advances

Investigation of magnetism and magnetic structure of anti-$ThCr_2Si_2$-type Tb_2O_2Bi by magnetization and neutron diffraction measurements

Cite as: AIP Advances **9**, 115301 (2019); https://doi.org/10.1063/1.5126399
Submitted: 02 September 2019 . Accepted: 16 October 2019 . Published Online: 08 November 2019

Hideyuki Kawasoko, Kenji Ohoyama, Ryosuke Sei, Kota Matsumoto, Daichi Oka, Akinori Hoshikawa, Toru Ishigaki, and Tomoteru Fukumura

Investigation of magnetism and magnetic structure of anti-$ThCr_2Si_2$-type Tb_2O_2Bi by magnetization and neutron diffraction measurements

Cite as: AIP Advances 9, 115301 (2019); doi: 10.1063/1.5126399
Submitted: 2 September 2019 • Accepted: 16 October 2019 •
Published Online: 8 November 2019

View Online Export Citation CrossMark

Hideyuki Kawasoko,[1] Kenji Ohoyama,[2] Ryosuke Sei,[1,3] Kota Matsumoto,[1] Daichi Oka,[1] Akinori Hoshikawa,[4] Toru Ishigaki,[4] and Tomoteru Fukumura[1,5]

AFFILIATIONS

[1] Department of Chemistry, Graduate School of Science, Tohoku University, Sendai 980-8578, Japan
[2] Graduate School of Science and Engineering, Ibaraki University, Tokai 319-1106, Japan
[3] Department of Chemistry, Graduate School of Science, The University of Tokyo, Tokyo 113-0033, Japan
[4] Frontier Research Center for Applied Atomic Sciences, Ibaraki University, Tokai 319-1106, Japan
[5] Advanced Institute for Materials Research and Core Research Cluster, Tohoku University, Sendai 980-8577, Japan

ABSTRACT

In this study, magnetization and neutron diffraction of anti-$ThCr_2Si_2$-type Tb_2O_2Bi polycrystals were measured at various temperatures. The magnetization cusp at 11.1 K was confirmed to correspond to antiferromagnetic ordering with a propagation vector of [0.5 0.5 0]. In addition, a metamagnetic behavior was observed below 5.0 K. The metamagnetic behavior could be attributed to the incommensurate magnetic structure with an anomaly at 5.0 K.

$ThCr_2Si_2$-type compounds composed of an alternative stack of Cr_2Si_2 block layer and Th monatomic square net have been investigated to explore their magnetic properties,[1–4] because both the transition metal at the Cr site and a rare earth metal at the Th site are responsible for the magnetic properties, resulting in complex magnetic phases.[5,6] On the other hand, anti-$ThCr_2Si_2$-type RE_2O_2Bi (RE = rare earth) is composed of an alternative stack of RE_2O_2 block layers and Bi square net, in which the former and the latter are responsible for electrical and magnetic properties, respectively.[7–9] Recently, RE_2O_2Bi has attracted attention because of its electrical properties such as metal-insulator transition and superconductivity.[10–15] However, the magnetic properties of RE_2O_2Bi were investigated by only magnetic susceptibility measurements, suggesting antiferromagnetic transition in RE_2O_2Bi (RE = Pr, Gd, Er).[10]

In this study, we elucidated magnetism and magnetic structure of Tb_2O_2Bi, whose crystal structure has only been reported,[9] by measuring magnetic properties and neutron diffraction. Tb_2O_2Bi was found to undergo an antiferromagnetic transition at 11.1 K with a propagation vector of [0.5 0.5 0]. In addition, metamagnetic behavior was observed below 5.0 K, probably associated with anomalies at 5.0 K of the magnetic susceptibility and the incommensurate peak of neutron diffraction.

Tb_2O_2Bi polycrystals were synthesized by the conventional solid-state reaction. Tb_4O_7 (99.9%) powder was heated at 1000 °C in a furnace for 10 h to remove moisture. Tb (99.9%), Tb_4O_7 (99.9%), and Bi (99.9%) powders were pelletized under 20 MPa in a nitrogen-filled glove box after mixing, where the nominal compositions were $Tb_2O_{1.6}Bi_{1.4}$ and $Tb_2O_{1.5}Bi_{1.5}$ for magnetization measurement and powder neutron diffraction, respectively. The pellets covered with Ta foil were sintered in evacuated quartz tubes at 500 °C for 7.5 h, followed by sintering at 1000 °C for 20 h. The sintered products were ground and pelletized under 30 MPa again in the glove box, and then the pellets covered with Ta foil were sintered in evacuated quartz tubes at 1000 °C for 10 h. The nominal composition was compensated to form the stoichiometric composition (Tb_2O_2Bi) by the evaporation of excess Bi and the additional oxidation during sintering, similar to the case of Y_2O_2Bi and Er_2O_2Bi.[11,12] Crystal and magnetic structures were evaluated by powder X-ray diffraction (D8 DISCOVER, Bruker AXS, Cu Kα radiation) and powder neutron diffraction at different temperatures (J-PARC, BL20, iMATERIA diffractometer). Rietveld analysis was performed by using RIETAN-FP (Ref. 16) and FullProf software (Ref. 17) to identify the crystal phases and the magnetic structure. Magnetization was evaluated by the magnetic property measurement system (MPMS, Quantum Design) at different temperatures and magnetic fields. The crystal structure was drawn with the VESTA.[18]

Figure 1(a) shows the temperature dependence of magnetic susceptibility in field cooling at 0.01 T. From the powder X-ray diffraction (Fig. S1) and its Rietveld analysis (Table S1), the sample was confirmed to be pure phase anti-$ThCr_2Si_2$-type Tb_2O_2Bi. The lattice constants of Tb_2O_2Bi were calculated as a = 3.8997(2) Å and

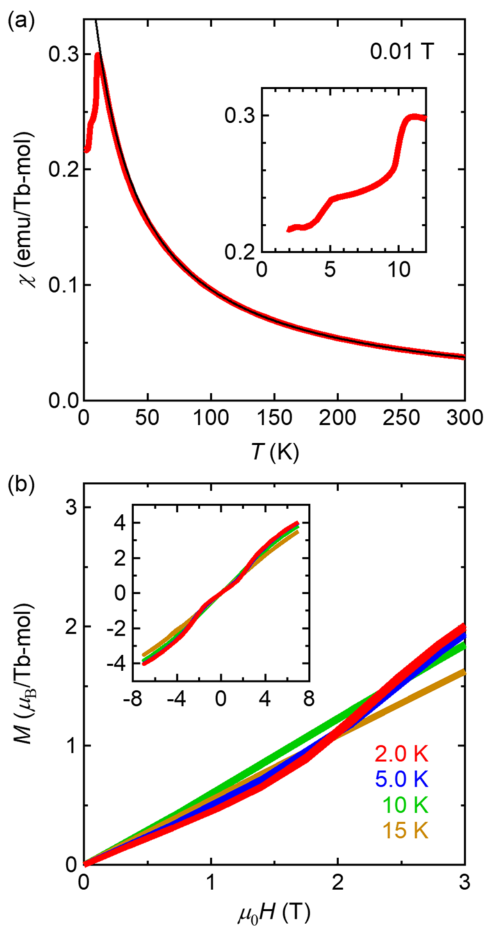

FIG. 1. (a) Temperature dependence of magnetic susceptibility for Tb_2O_2Bi. Black curve indicates the fitting result of the Curie-Weiss law. Inset shows the magnified plot. (b) Magnetization curves of Tb_2O_2Bi at various temperatures. Inset shows the full range of magnetization curves.

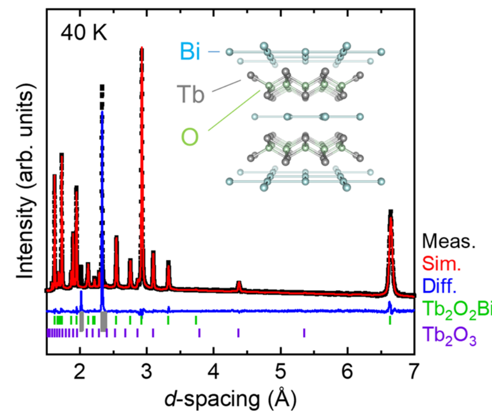

FIG. 2. Neutron diffraction pattern of Tb_2O_2Bi at 40 K. Inset shows the crystal structure of Tb_2O_2Bi. Black, red, and blue lines indicate measurement pattern, simulation pattern, and their difference, respectively. Green and purple bars indicate the nuclear reflection positions of Tb_2O_2Bi and Tb_2O_3 phases, respectively. Gray areas (d-spacing = 1.99–2.04 and 2.31–2.36 Å) with only Al peaks from sample cells were excluded in the process of Rietveld analysis.

c = 13.3261(7) Å, similar to the previous study at 298 K (a = 3.896 Å and c = 13.317 Å).[9] The magnetic susceptibility increased with decreasing temperature with a clear kink at T_N = 11.1 K originating from antiferromagnetic ordering of Tb_2O_2Bi, as described below. Such a kink structure was also observed in Pr_2O_2Bi, Gd_2O_2Bi, and Er_2O_2Bi polycrystals at T_N =15.0 K, 10.1 K, and 3.0 K, respectively, being attributed to antiferromagnetic transition from the magnetization measurements.[10] Below the antiferromagnetic transition temperature of Tb_2O_2Bi, an additional anomaly was observed at T_m = 5.0 K. From the Curie-Weiss fitting at high temperatures, the effective Bohr magneton value P_{eff} was 9.86 μ_B close to theoretical value 9.72 μ_B for Tb^{3+} ($4f^8$), confirming the trivalent state of Tb cation like other RE cations in RE_2O_2Bi (RE = Pr, Gd, Er).[10]

Figure 1(b) shows the magnetization curves of Tb_2O_2Bi at low temperatures. The linear magnetic field dependence was observed at 10 K and 15 K, while the nonlinear increases were observed around 1.5 T at 2.0 K and 5.0 K, indicating metamagnetic behaviors. These nonlinear behaviors below 5.0 K could be related to the anomaly at

TABLE I. Results of Rietveld analysis for the neuron diffraction pattern of Tb_2O_2Bi at 40 K (R_{wp}: R-factor; R_{exp}: expected R-factor; and χ^2: Chi-squared value).

Sample	Tb_2O_2Bi
Space group	$I4/mmm$
a (Å)	3.892 55(2)
c (Å)	13.292 37(13)
V (Å^3)	201.405(2)
Tb z	0.334 02(7)
Fraction (mol %)	79.64
R_{wp}	5.39
R_{exp}	1.52
χ^2	12.5

T_m = 5.0 K in the magnetic susceptibility curve [Fig. 1(a)]. Interestingly, these two kinds of magnetic transitions were observed in $ThCr_2Si_2$-type Tb compounds such as $TbNi_2Si_2$ (T_N = 14.6 K and T_m = 7.6 K), $TbNi_2Ge_2$ (T_N = 16.7 K and T_m = 9.6 K), and $TbCu_2Si_2$ (T_N = 11.9 K and T_m = 9.1 K) despite different crystallographic positions of Tb.[19–22]

In order to confirm the magnetic structure of Tb_2O_2Bi, the neutron diffraction was measured at 3.6 K and 40 K around those magnetic transition temperatures. Figure 2 shows the neutron diffraction pattern at 40 K. From the Rietveld analysis (Table I), anti-$ThCr_2Si_2$-type Tb_2O_2Bi was confirmed as the main phase (79.64 mol %), in addition to the Tb_2O_3 secondary phase (20.46 mol %). The lattice constants of Tb_2O_2Bi were calculated as a = 3.892 55(2) Å and c = 13.292 37(13) Å. All peaks were generated by the nuclear reflection of Tb_2O_2Bi and Tb_2O_3, indicating no magnetic ordering at 40 K.

Figure 3(a) shows the neutron diffraction pattern at 3.6 K. Lattice constants of Tb_2O_2Bi were calculated to be a = 3.891 98(11) Å and c = 13.291 21(61) Å, suggesting thermal contraction without structural transition from 40 K. In addition to the nuclear reflection of Tb_2O_2Bi, magnetic components were observed at 3.6 K, in which all sharp peaks of the magnetic reflections can be attributed to antiferromagnetic ordering with a propagation vector, k = [0.5 0.5 0]. Hence, T_N = 11.1 K corresponds to the Néel temperature, at which a kink was observed in magnetic susceptibility in Fig. 1(a). The broad peaks around d-spacing of 4.5 Å and 6.0 Å were not explained by the propagation vector [0.5 0.5 0], suggesting the development of unknown incommensurate magnetic structures. It is noted that these magnetic reflections are not related to the antiferromagnetic transition of Tb_2O_3 at 2 K.[23] Representational analysis of space group $I4/mmm$ with this propagation vector suggests three candidates of the magnetic structure of Tb_2O_2Bi, as illustrated in the insets of Figs. 3(a)–3(c), whose basis vectors are [1 −1 0], [−1 1 0]; [1 1 0], [−1 −1 0]; and [0 0 1], [0 0 −1], respectively.[24–28] Among them, the magnetic structure with [1 −1 0] and [−1 1 0] in Fig. 3(a) was best fitted by refining the parameters of the magnetic structure at 3.6 K using the Rietveld analysis (Table II).

Figure 4 shows the temperature dependence of the peak intensity of magnetic reflections below T_N = 11.1 K. The peak intensities of (0.5 0.5 1) and (0.5 0.5 2) monotonically increased with decreasing temperature below T_N = 11.1 K, indicating the development of antiferromagnetic ordering in Tb_2O_2Bi. On the other hand, the peak intensity of the incommensurate magnetic structure around d-spacing = 4.5 Å as described in Fig. 4 showed a discontinuity around 5 K. This behavior could be related to anomaly at 5.0 K in magnetic susceptibility, suggesting that the metamagnetic behavior was caused by the incommensurate magnetic structure in Tb_2O_2Bi, as was observed in $TbNi_2Si_2$, $TbNi_2Ge_2$, and $TbCu_2Si_2$.[20–22]

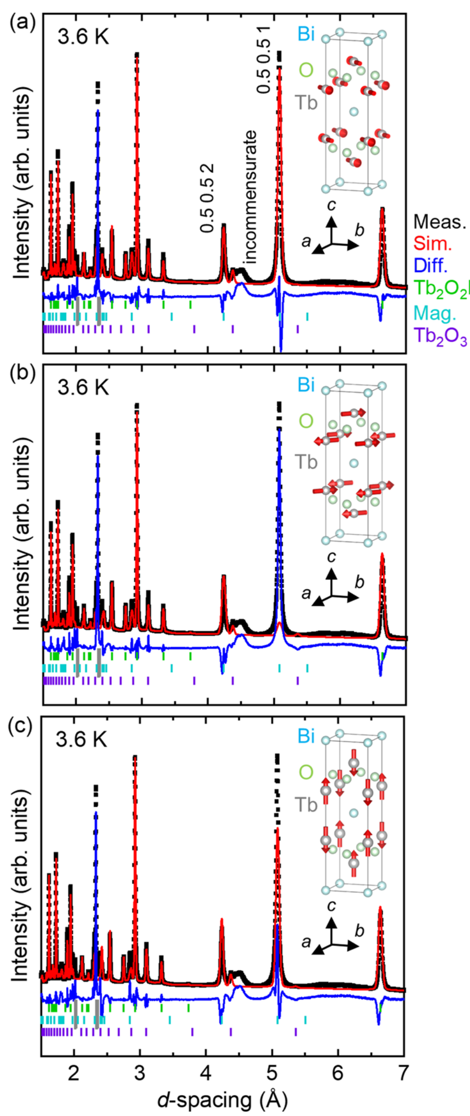

FIG. 3. Neutron diffraction patterns of Tb_2O_2Bi at 3.6 K and the Rietveld refinements for basis vectors of (a) [1 −1 0], [−1 1 0]; (b) [1 1 0], [−1 −1 0]; and (c) [0 0 1], [0 0 −1]. Plot style is the same as that of Fig. 1. Light blue bars denote the magnetic reflection positions of the Tb_2O_2Bi phase. Gray areas (d-spacing = 2.00–2.03 and 2.31–2.36 Å) with only Al peaks from sample cells were excluded in the process of Rietveld analysis.

TABLE II. Results of Rietveld analysis for the neuron diffraction pattern of Tb_2O_2Bi at 3.6 K (R_{wp}: R-factor; R_{exp}: expected R-factor; and χ^2: Chi-squared value).

Basis vectors	[1 −1 0], [−1 1 0]	[1 1 0], [−1 −1 0]	[0 0 1], [0 0 −1]
Sample	Tb_2O_2Bi	Tb_2O_2Bi	Tb_2O_2Bi
Space group	$I4/mmm$	$I4/mmm$	$I4/mmm$
a (Å)	3.891 98(11)	3.891 80(20)	3.892 03(14)
c (Å)	13.291 21(61)	13.293 53(105)	13.292 25(79)
V (Å^3)	201.329(8)	201.345(14)	201.350(11)
Tb z	0.337 49(27)	0.333 76(54)	0.335 92(41)
Fraction (mol %)	76.56	75.82	75.67
R_{wp}	24.2	42.2	31.6
R_{exp}	1.18	1.18	1.18
χ^2	418	1270	713

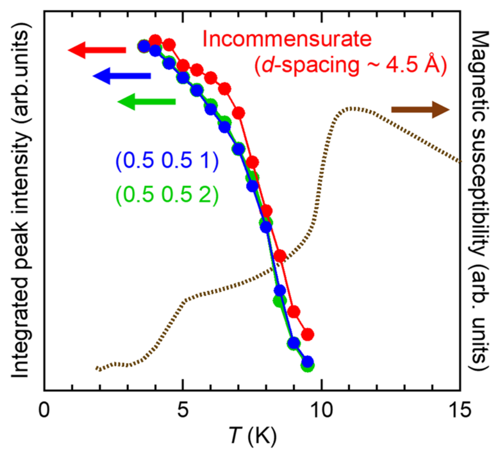

FIG. 4. Temperature dependence of integrated intensity of (0.5 0.5 1), (0.5 0.5 2) and incommensurate peaks around *d*-spacing = 4.5 Å. Temperature dependence of magnetic susceptibility in Fig. 2(a) (dotted line) is also shown.

In summary, anti-$ThCr_2Si_2$-type Tb_2O_2Bi was found to show antiferromagnetic ordering and metamagnetic behavior below T_N = 11.1 K and T_m = 5.0 K, respectively. Neutron diffraction measurements indicated that a propagation vector of antiferromagnetic ordering was [0.5 0.5 0] where basis vectors corresponded to [1 −1 0] and [−1 1 0]. The incommensurate magnetic structure with an anomaly at 5.0 K was also observed below T_N, being the possible origin of metamagnetic behavior in Tb_2O_2Bi.

See the supplementary material for the X-ray diffraction pattern of Tb_2O_2Bi used for the magnetization measurement.

This study was in part supported by JSPS KAKENHI (Grant Nos. 26105002 and 16H06441), JST-CREST, and Yazaki Memorial Foundation for Science and Technology. The neutron experiments at the Materials and Life Science Experimental Facility of the J-PARC were performed under a user program (Proposal No. 2017A0117).

REFERENCES

[1] I. Felner and I. Mayer, "Magnetic ordering in rare earth iron silicides and germanides of the RFe_2X_2 Type," Solid State Commun. **16**, 1005 (1975).
[2] A. Szytuta and I. Szott, "Magnetic properties of ternary RMn_2Si_2 and RMn_2Ge_2 compounds," Solid State Commun. **40**, 199 (1981).
[3] I. Felner and I. Nowik, "Local and itinerant magnetism and crystal structure of RRh_2Ge_2 and RRu_2Ge_2 (R = rare earth)," J. Phys. Chem. Solids **46**, 681 (1985).
[4] M. Reehuis and W. Jeitschko, "Structure and magnetic properties of the phosphide $CaCo_2P_2$ and LnT_2P_2 with $ThCr_2Si_2$ structure and LnTP with PbFCl structure (Ln = lanthanoids, T = Fe, Co, Ni)," J. Phys. Chem. Solids **51**, 961 (1990).
[5] J. L. Wang, S. J. Kennedy, S. J. Campbell, M. Hofmann, and S. X. Dou, "Phase gap in pseudoternary $R_{1-y}R'_yMn_2X_{2-x}X'_x$ compounds," Phys. Rev. B **87**, 104401 (2013).
[6] X. Tan, Z. P. Tener, and M. Shatruk, "Correlating itinerant magnetism in RCo_2Pn_2 pnictides (R = La, Ce, Pr, Nd, Eu, Ca; Pn = P, As) to their crystal and electronic structures," Acc. Chem. Res. **51**, 230 (2018).
[7] R. Benz, "Ce_2O_2Sb and Ce_2O_2Bi crystal structure," Acta Crystallogr., Sect. B: Struct. Crystallogr. Cryst. Chem. **27**, 853 (1971).
[8] J. Nuss and M. Jansen, "Syntheses, structures and properties of the pnictide oxides R_2PnO_2 (R = Ce, Pr; Pn = Sb, Bi)," J. Alloys Compd. **480**, 57 (2009).
[9] J. Nuss and M. Jansen, "On the rare earth metal bismuthide oxides RE_2BiO_2 (RE = Nd, Tb, Dy, Ho)," Z. Anorg. Allg. Chem. **638**, 611 (2012).
[10] H. Mizoguchi and H. Hosono, "A metal-insulator transition in R_2O_2Bi with an unusual Bi^{2-} square net (R = rare earth or Y)," J. Am. Chem. Soc. **133**, 2394 (2011).
[11] R. Sei, S. Kitani, T. Fukumura, H. Kawaji, and T. Hasegawa, "Two-dimensional superconductivity emerged at monatomic Bi^{2-} square net in layered Y_2O_2Bi via oxygen incorporation," J. Am. Chem. Soc. **138**, 1085 (2016).
[12] K. Terakado, R. Sei, H. Kawasoko, T. Koretsune, D. Oka, T. Hasegawa, and T. Fukumura, "Superconductivity in anti-$ThCr_2Si_2$-type Er_2O_2Bi induced by incorporation of excess oxygen with CaO oxidant," Inorg. Chem. **57**, 10587 (2018).
[13] R. Sei, T. Fukumura, and T. Hasegawa, "Reductive solid phase epitaxy of layered Y_2O_2Bi with Bi^{2-} square net from (Y, Bi) powders and Y_2O_3 amorphous thin film," Cryst. Growth Des. **14**, 4227 (2014).
[14] R. Sei, T. Fukumura, and T. Hasegawa, "2D electronic transport with strong spin–orbit coupling in Bi^{2-} square net of Y_2O_2Bi thin film grown by multilayer solid-phase epitaxy," ACS Appl. Mater. Interfaces **7**, 24998 (2015).
[15] S. Shibata, R. Sei, T. Fukumura, and T. Hasegawa, "Magnetic and magnetotransport properties of $ThCr_2Si_2$-type Ce_2O_2Bi composed of conducting Bi^{2-} square net and magnetic Ce-O layer," Appl. Phys. Lett. **110**, 192410 (2017).
[16] F. Izumi and K. Momma, "Three-dimensional visualization in powder diffraction," Solid State Phenom. **130**, 15 (2007).
[17] J. Rodríguez-Carvajal, "Recent advances in magnetic structure determination by neutron powder diffraction," Physica B **192**, 55 (1993).
[18] K. Momma and F. Izumi, "VESTA 3 for Three-dimensional visualization of crystal, volumetric and morphology data," J. Appl. Crystallogr. **44**, 1272 (2011).
[19] J. M. Barandiaran, D. Gignoux, D. Schmitt, J. C. Gomezsal, and J. Rodriguez Fernandez, "Magnetic properties of RNi_2Si_2 compounds (R= rare earth)," J. Magn. Magn. Mater. **69**, 61 (1987).
[20] T. Shigeoka, H. Fujii, M. Nishi, Y. Uwatoko, T. Takabatake, I. Oguro, K. Motoya, N. Iwata, and Y. Ito, "Metamagnetism in $TbNi_2Si_2$ single crystal," J. Phys. Soc. Jpn. **61**, 4559 (1992).
[21] Z. Islam, C. Detlefs, A. I. Goldman, S. L. Bud'ko, P. C. Canfield, J. P. Hill, D. Gibbs, T. Vogt, and A. Zheludev, "Neutron diffraction and X-ray resonant exchange-scattering studies of the zero-field magnetic structures of $TbNi_2Ge_2$," Phys. Rev. B **58**, 8522 (1998).
[22] T. Shigeoka, M. Tanaka, T. Fujiwara, and Y. Uwatoko, "Complex magnetic phase diagrams of $TbCu_2Si_2$ single crystal," J. Phys.: Conf. Ser. **200**, 032065 (2010).
[23] J. B. MacChesney, H. J. Williams, R. C. Sherwood, and J. F. Potter, "Preparation and low temperature magnetic properties of the terbium oxides," J. Chem. Phys. **44**, 596 (1966).
[24] E. F. Bertaut, "Lattice theory of spin configuration," J. Appl. Phys. **33**, 1138 (1962).
[25] E. F. Bertaut, "Representation analysis of magnetic structures Acta," Acta Crystallogr., Sect. A: Cryst. Phys., Diffr., Theor. Gen. Crystallogr. **A24**, 217 (1968).
[26] E. F. Bertaut, "Magnetic structure analysis and group theory," J. Phys. Colloq. **C1**, 462 (1971).
[27] E. F. Bertaut, "On group theoretical techniques in magnetic structure analysis," J. Magn. Magn. Mater. **24**, 267 (1981).
[28] A. S. Wills, "A new protocol for the determination of magnetic structures using simulated annealing and representational analysis (SARA*h*)," Physica B **276**, 680 (2000).